Accurate Measurement of Electron Beam Induced Displacement Cross Sections for Single-Layer Graphene

Jannik C. Meyer,[1,2,*] Franz Eder,[2] Simon Kurasch,[1] Viera Skakalova,[3,2] Jani Kotakoski,[4,2] Hye Jin Park,[3] Siegmar Roth,[3,5] Andrey Chuvilin,[1,6] Sören Eyhusen,[7] Gerd Benner,[7] Arkady V. Krasheninnikov,[4,8] and Ute Kaiser[1,†]

[1]*Central Facility for Electron Microscopy, Group of Electron Microscopy of Materials Science, University of Ulm,
Albert Einstein Allee 11, 89081 Ulm, Germany*
[2]*University of Vienna, Department of Physics, Boltzmanngasse 5, 1090 Vienna, Austria*
[3]*Max Planck Institute for Solid State Research, Heisenbergstrasse 1, 70569 Stuttgart, Germany*
[4]*Department of Physics, University of Helsinki, P.O. Box 43, 00014 Helsinki, Finland*
[5]*WCU Flexible Electronics, School of Electrical Engineering, Korea University, Seoul, Korea*
[6]*CIC nanoGUNE Consolider, Avenida de Tolosa 76, 20018, San Sebastian, Spain and Ikerbasque,
Basque Foundation for Science, 48011, Bilbao, Spain*
[7]*Carl Zeiss NTS GmbH, Carl-Zeiss-Strasse 56, 73447 Oberkochen, Germany*
[8]*Department of Applied Physics, Aalto University, P.O. Box 1100, 00076 Aalto, Finland*
(Received 18 January 2012; published 7 May 2012)

We present an accurate measurement and a quantitative analysis of electron-beam-induced displacements of carbon atoms in single-layer graphene. We directly measure the atomic displacement ("knock-on") cross section by counting the lost atoms as a function of the electron-beam energy and applied dose. Further, we separate knock-on damage (originating from the collision of the beam electrons with the nucleus of the target atom) from other radiation damage mechanisms (e.g., ionization damage or chemical etching) by the comparison of ordinary (^{12}C) and heavy (^{13}C) graphene. Our analysis shows that a static lattice approximation is not sufficient to describe knock-on damage in this material, while a very good agreement between calculated and experimental cross sections is obtained if lattice vibrations are taken into account.

Radiation damage is one of the key limitations of high-resolution transmission electron microscopy (HRTEM) [1]. In particular, the continuous improvements in instrumental resolution [2,3] inevitably entail increased doses per area that need to be applied to a sample. The need for high doses is further increased for new techniques such as single-atom or single-atomic-column spectroscopy [4–7], atomic resolution electron tomography [8], or the analysis of charge distributions from very high signal-to-noise ratio HRTEM images [9]. For light element materials, such as carbon nanotubes [10,11], fullerenes [12], graphene [13,14], boron nitride [15,16], and probably many more, the dose limitation is particularly severe for three reasons. First, it is obvious, that knock-on damage cross sections will be higher for low atomic number elements [17]. Second, the light elements produce less contrast than heavier elements, so that even higher doses are needed to obtain a sufficient signal-to-noise ratio. And third, most of the novel materials from light elements, such as graphene or carbon nanotubes, appear in the form of low dimensional allotropes that have only one or a few atoms in a typical projection of a high-resolution image. While almost all atomic spacings can in principle be resolved by the currently available instrumentation, the question remains whether a sample is stable under the beam until an image has been acquired. In spite of a wide range of previous studies concerning irradiation damage in carbon nanostructures [17–24], a quantitative experimental determination of atomic displacement cross sections for this important class of materials is absent. In fact, only very few quantitative measurements of electron-beam-induced displacement cross sections [25,26] (beyond damage threshold measurements [27,28]) can be found in the literature. The understanding of irradiation effects is also important for targeted irradiation-induced modifications of a material: For the case of graphene, for example, a controlled introduction of vacancies and nonhexagonal rings may lead to derived sp^2 hybridized carbon sheets with specific properties [29–34].

Here, we present an extensive measurement and analysis of electron-beam-induced displacements. We directly count the number of ejected atoms under irradiation as functions of dose, dose rate, and electron energy. Suspended single-layer graphene sheets provide the perfect test sample for this analysis: They can be prepared in a precisely defined geometry (1 atomic layer thick, hexagonal lattice, with practically no defects initially), are relatively easy to model, and the number of ejected atoms in multivacancy configurations can be directly obtained from HRTEM images [33,35]. Under 80 keV electron irradiation, the defect free graphene lattice remains undisturbed up to very high doses [9,35] but knock-on damage begins already a few keV above this energy [17–24]. Importantly, for energies near the knock-on threshold, the changes in the lattice occur slowly, so that the appearance and growth of

multivacancies can be directly observed in real time. In this way, we can count the number of lost atoms as a function of applied dose and for different acceleration voltages, hence providing a direct measurement of the knock-on cross section.

We present insights from a tremendous data set that was obtained for the purpose of quantitating the radiation damage in graphene. We have obtained and analyzed image sequences as shown in Fig. 1 for many acceleration voltages (80, 90, 95, 100 kV), and for both, the ^{12}C "normal" graphene sample and isotope-enriched ^{13}C "heavy graphene" samples. For all of this data, the defect configurations were analyzed at different doses of exposure, and the number of missing atoms was counted (see Supplemental Material [36] for further examples from the data set). We also studied ^{12}C graphene under 20 keV electron irradiation [37], in order to obtain a further distinction between knock-on damage and other effects such as chemical etching or radiolysis.

Experimentally, we prepared graphene membranes by mechanical exfoliation and transfer to TEM grids as described previously [38], and by chemical vapor deposition (CVD) followed by transfer to TEM grids, as described in Ref. [39]. We assume that these samples contain the natural
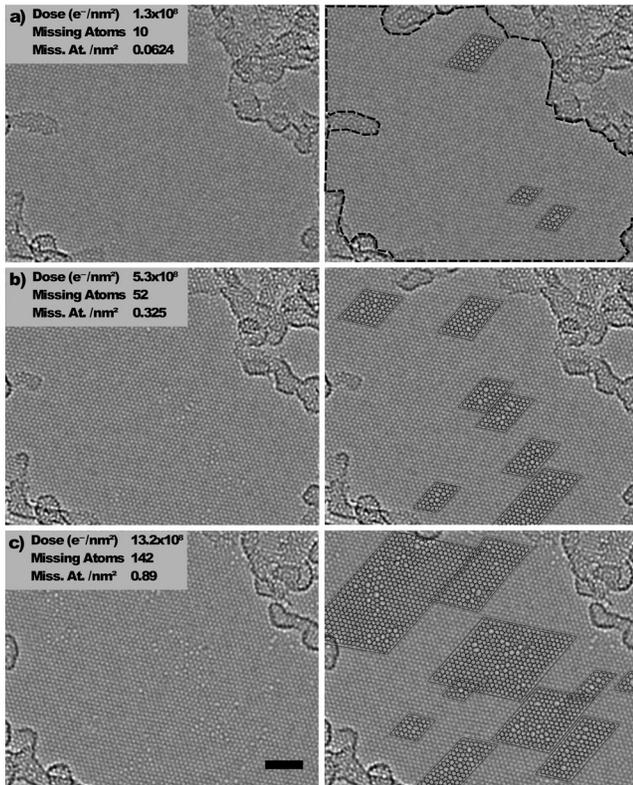

FIG. 1. Multivacancy defects with increasing dose under 100 keV observation of ^{12}C graphene (a)–(c). Images are shown without (left) and with overlay of the atomic configuration (right). The dashed line in (a) indicates the area that is used to calculate the missing atoms per area. The scale bar is 2 nm.

isotope composition in carbon, which is 98.9% ^{12}C and 1.1% ^{13}C. In addition, we synthesized "heavy graphene" samples made from ^{13}C, by CVD. The synthesis recipe for the ^{13}C graphene followed the same procedure as we described in Ref. [39], except that the standard methane precursor was replaced by 99% ^{13}C enriched methane (purchased from Sigma-Aldrich). We aligned an image-side aberration-corrected FEI Titan 80–300 for HRTEM imaging at 80, 90, 95, and 100 kV, hence providing a closely spaced series around the threshold voltage [20]. The spherical aberration was set to ca. 20 μm and images were recorded at Scherzer defocus. Under these conditions, dark contrast can be directly interpreted in terms of the atomic structure. For 20 kV imaging, we used an image-side aberration-corrected Zeiss Libra as described in Ref. [37]. In all experiments, long image sequences of the graphene samples were recorded (see videos in the Supplemental Material [36]), typically consisting of $\sim$100 images with 1 s exposures recorded at 2–4 s intervals and typical dose rates of $10^6 \frac{e^-}{nm^2 \cdot s}$. The sample is under continuous irradiation, only the beam shutter behind the sample is used. We analyze the creation and the increase in the density of vacancies and multivacancies in the image sequences. This approach was feasible up to ca. 100 kV, while at 120 kV the damage occurred too quickly compared to the time or dose needed to acquire an HRTEM image with a sufficient signal-to-noise ratio.

Example images (for 100 kV, ^{12}C) are shown in Fig. 1. The left-hand side shows images from an image sequence recorded at 100 kV and the right-hand side shows the same images with a structure overlay of the atomic configuration. The analysis of such atomic configurations has been described in more detail previously [33,35]: the multivacancies reconstruct into configurations that involve primarily carbon pentagons, heptagons, and octagons as well as other nonhexagonal rings, and can be well assigned from HRTEM data. For counting the atoms, we draw a supercell around the defect clusters, such that the boundary of this cell does not intersect any defect (see Fig. 1). Moreover, the supercell must not contain unpaired dislocation cores, which can be easily verified by counting the number of unit cells on opposing sides of the parallelogram. We then calculate the number of atoms that should be within this cell for the defect free case, and compare it to the number of atoms actually present.

The results of this assessment are shown in Fig. 2, where the number of lost atoms vs total dose per area is shown for all experiments. A linear fit is made for each case, and the slope directly provides the experimental knock-on cross section (since a small initial damage may be created before the first image is recorded some of the lines do not go through the origin). Two independent measurements were made for the 100 kV case, but with a 3$\times$ different *dose rate* ($3.5 \times 10^5 \frac{e^-}{nm^2 s}$ and $1 \times 10^6 \frac{e^-}{nm^2 s}$). From the nearly identical result, we can exclude a dose rate effect within
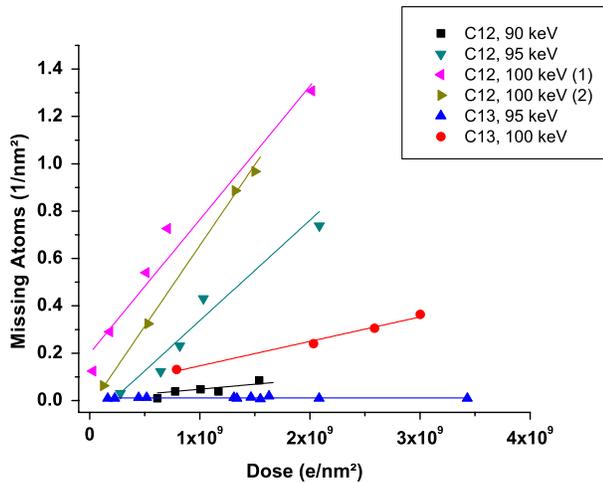
FIG. 2 (color online).   Number of displaced atoms vs dose and electron energy. For the 100 keV case, two different dose rates were compared, with (2) having a ca. $3\times$ higher dose rate than (1).

FIG. 3.   Atomic displacements (knock-on damage) vs chemical etching. The comparison between ^{12}C and ^{13}C graphene shows that the formation of vacancies within the pristine lattice is a direct knock-on damage effect ($a + b$, ^{12}C, and ^{13}C sample after a dose of 1.4×10^9 $\frac{e^-}{nm^2}$ at 95 keV). In contrast, the formation of extended holes in graphene is always induced by contamination on the sheet [(c), initial image, and (d) after exposure to ca. 10^9 $\frac{e^-}{nm^2}$], and the damage rate depends on the vacuum levels. Dashed circles in (c) and (d) denote same areas. (e) Image sequence showing the growth of holes in graphene at 20 keV (example shown for a bilayer area). Scale bars are 2 nm (a)–(d) and 5 nm (e).

our experimental precision. Under 80 keV irradiation (not shown in Fig. 2), no vacancies were formed in pristine areas up to very high doses (beyond 10^{10} $\frac{e^-}{nm^2}$).

We begin our discussion by pointing out the clear difference between the ^{12}C and ^{13}C graphene membranes, and the differences between knock-on damage and a chemical etching effect. We find that the generation of vacancies within initially pristine, clean, and defect free graphene membranes depends on the acceleration voltage, and also on the isotope composition (^{12}C vs ^{13}C). Figures 3(a) and 3(b) show graphene membranes of the two isotopes after exposure to 95 keV electrons, where the difference is most clearly visible. Hence, this must be a result of a direct collision between a beam electron and the carbon nucleus: Any chemical effect, or ionization damage, would not distinguish between ^{12}C and ^{13}C. As a side remark, we note that graphene membranes made from ^{13}C might provide an even better TEM sample support than ordinary single-layer graphene: The contrast background in HRTEM is identical, but the radiation damage rate is lower.

However, in contrast to the vacancy formation, the growth of extended holes in graphene [40] is not predominantly a knock-on damage effect: We found that the growth rate of holes in graphene only weakly depends on the electron energy on a wide range of 20 to 100 keV. Holes still form and grow in graphene under 20 keV irradiation [Figs. 1(c)–1(e)], and may even grow faster at low voltages (see Supplemental Material [36]). This is in stark contrast to expectations from knock-on damage, where the threshold for displacing edge atoms is expected to be near 50 keV [41]. As shown in Figs. 3(c) and 3(d), the extended holes always nucleate at contamination sites. We noticed that their growth rate is related to the vacuum levels, which varied in the range of 10^{-6} to 10^{-7} mbar, e.g., with use of the cold trap in the column, the time after insertion of the sample, or different outgassing rates of different sample
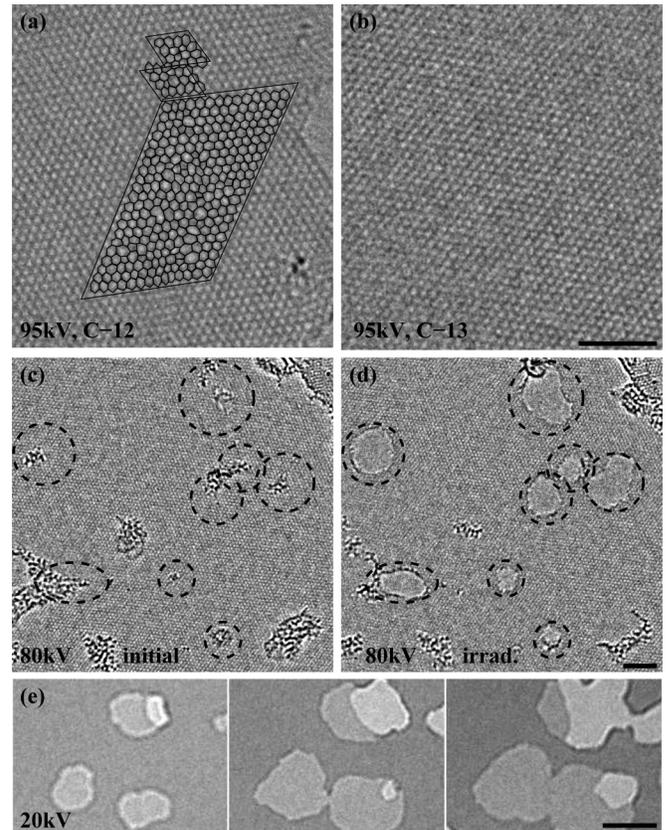
holders. We conclude that this is beam-induced etching with residual water or oxygen in the system as described in Refs. [23,42]. Therefore, we count the formation of vacancies in initially clean and defect free areas as knock-on effect, but do not take into account the extended holes that nucleate at contamination sites.

The analysis of our results culminates in the plot shown in Fig. 4. Here, each of the slopes from Fig. 2 provides one data point for a measured displacement cross section. The error bars indicate the statistical variation (standard deviation) in the data. Also shown in Fig. 4 are calculated curves from existing and new calculations that will be discussed below. For two curves, we show a shaded area between $1\times$ and $2\times$ the calculated cross section, since correlated sputtering of carbon atoms may increase the observed atom loss by up to a factor of 2. After creation of a monovacancy
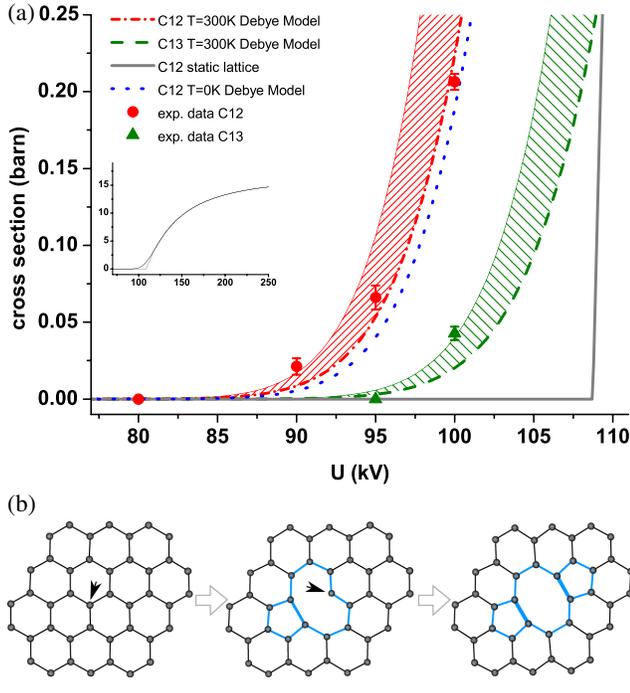
FIG. 4 (color online).   (a) Measured and calculated knock-on displacement cross sections. The lower boundary of the shaded areas correspond to the calculated cross section, while the upper boundary is twice the calculated value (as would be expected for correlated sputtering). The inset shows the calculations for ^{12}C, 300 K and static lattice on a larger energy range. (b) Correlated displacement of carbon atoms. After creation of a monovacancy, one carbon atom remains with a dangling bond and a much lower emission threshold. Subsequent sputtering of this atom may effectively double the cross section.

by electron impact, one carbon atom is left with a dangling bond and a much lower emission threshold [21,41]. Subsequent (and much more rapid) sputtering of this atom may effectively double the rate of atom loss [Fig. 4(b)]. As a competing mechanism, two monovacancies that are created close to each other may combine and form a stable divacancy (since impacts of energetic electrons can rotate bonds in graphene [33,43], it is likely that exposure to the beam increases also the diffusivity of vacancies). In this case, the sputtering rate would not have to be doubled. Qualitatively, one would expect that correlated sputtering is dominant close to the threshold, while nearby monovacancies are more likely generated at higher electron energies (this is further discussed in the Supplemental Material [36]). In any case, the resulting multivacancy configurations contain only very few under-coordinated carbon atoms, while the 3-coordinated atoms in the reconstructed configurations are expected to have an emission threshold similar to that of an atom in the pristine graphene sheet [43]. Another conceivable mechanism that might have an influence on the experimental results, namely, the annealing of vacancies with mobile carbon

adatoms, can not be dominant in our experiment as evidenced by the absence of a dose rate effect. Hence, we expect a rate of atom loss in-between $1\times$ and $2\times$ of the value calculated for pristine graphene.

The cross section for Coloumb scattering between an electron and a corresponding target nucleus was derived by Mott [44]. McKinley and Feshbach have found an analytic expression for the Mott scattering cross section as a function of the maximum transferred energy [45],

$$
\sigma_D = \frac{4Z^2 E_R^2}{m_e^2 c^4}\left(\frac{T_{\max}}{T_{\mathrm{thr}}}\right)\pi a_0^2\left(\frac{1-\beta^2}{\beta^4}\right)\left\{1 + 2\pi\alpha\beta\sqrt{\frac{T_{\mathrm{thr}}}{T_{\max}}}\right.
$$
$$
\left. - \frac{T_{\mathrm{thr}}}{T_{\max}}\left[1 + 2\pi\alpha\beta + (\beta^2 + \pi\alpha\beta)\ln\left(\frac{T_{\max}}{T_{\mathrm{thr}}}\right)\right]\right\}, \quad (1)
$$

where Z is the atomic number of the target atoms, $E_R = 13.6$ eV the Rydberg energy, $a_0 = 5.3 \times 10^{-11}$ m the Bohr radius of the hydrogen atom, $\beta = \frac{v_e}{c}$ (electron velocity v_e divided by the speed of light c), m_e the mass of the electron and $\alpha \approx \frac{Z}{137}$. $T_{\max}$ represents the maximum transferred energy in the collision event and T_{thr} a threshold energy for atomic displacement. Without modifications, Eq. (1) is suitable to evaluate the total "knock-on" cross section for an atom at rest with a given ejection threshold energy. The curve from Eq. (1) ("static lattice" in Fig. 4), features a rather sharp onset of radiation damage with increasing acceleration voltage: The cross section is zero up to a well defined threshold (here 108 kV), and then rises to several barn (beyond all our measured values) only a few kV above this threshold. Changing the displacement threshold in the McKinley-Feshbach formula predominantly shifts this curve sideways, but does not affect the sharp onset. Hence, independent of the free parameter T_{thr} this approximation is in clear contrast to our experiment, which shows a smooth onset of the damage cross section between 80 and 100 keV.

Remarkably, our data can be explained by considering the effect of the struck atom's vibrations on its own displacement. While the effect has been discussed earlier [28,46,47], our measurement provides precise experimental evidence of this intriguing effect. In essence, it means that an atom that is struck by an electron while it happens to move parallel to the electron beam can obtain a higher maximum transferred energy $T_{\max}$ than if it were static. For our calculation, we approximate the phonon distribution of the material in the framework of the Debye model. We use the Debye temperature calculated for out of plane vibrations in graphene of $\theta_D = 1287$ K from Ref. [48]. Since θ_D depends on the speed of sound, it follows for the Debye temperature of ^{13}C that $\theta_D^{13} = \sqrt{\frac{12}{13}}\theta_D^{12}$. We extract the distribution of atom velocities in the beam direction from the model, calculate the maximum transferred energy $T_{\max}(v, E)$ as a function of the atom velocity v and electron energy E, and obtain the weighted sum of the sputtering cross section numerically (see Supplemental Material

[36]). In other words, we still use the Mott scattering cross section, but we consider that the atom is not at rest initially. The threshold energy of $T_{thr} = 22$ eV was taken from first principles calculations [49] without any adjustments (Refs. [21,22] give similar values). With this value, the smooth onset of knock-on damage between 80–100 keV is very well reproduced. For the first time, no adjustment to the calculated threshold energy T_{thr} is needed to explain the data, as was the case in previous studies [22,49]. Remarkably, the previous mismatch between theory and experiments was not due to inadequate calculations of T_{thr}, but because the effects of lattice vibrations on the elastic collision were not considered. Interestingly, the calculated curves are almost identical for the zero-Kelvin and room-temperature case (Fig. 4, ^{12}C $T = 0$ K and $T = 300$ K curves). This implies that already the zero-point energy of the phonon modes is sufficient to explain the increased sputtering cross section as compared to the static lattice.

In summary, we have made an accurate measurement of atomic displacement cross sections for carbon atoms in single-layer graphene. The cross section smoothly rises from practically zero (10^{-4} barn) at 80 keV to ~ 0.2 barn at 100 keV. In practice this means that 80 keV imaging of defect free graphene is easily possible, while already 100 keV TEM images might not represent the original configuration of a sample. A static lattice model is not sufficient to model the process, and the contribution of atomic motion adds significantly to knock-on damage cross sections near the threshold. The difference between ^{12}C and ^{13}C isotopes is detectable and further confirms the model. While the results on graphene will be important for HRTEM studies of this material and related ones (especially carbon nanotubes), the generalized insights to radiation damage mechanisms should be more generally applicable to any material where knock-on damage is important. Our results show that knock-on displacement cross sections can be modeled with high accuracy, if lattice vibrations are taken into account.

---

*Corresponding author.
jannik.meyer@univie.ac.at
†Corresponding author.
ute.kaiser@uni-ulm.de

[1] R. F. Egerton, P. Li, and M. Malac, Micron **35**, 399 (2004).

[2] M. Haider, S. Uhlemann, E. Schwan, H. Rose, B. Kabius, and K. Urban, Nature (London) **392**, 768 (1998).

[3] P. E. Batson, N. Dellby, and O. L. Krivanek, Nature (London) **418**, 617 (2002).

[4] P. E. Batson, Nature (London) **366**, 727 (1993).

[5] U. Kaiser, D. A. Muller, J. L. Grazul, A. Chuvilin, and M. Kawasaki, Nature Mater. **1**, 102 (2002).

[6] D. A. Muller, L. F. Kourkoutis, M. Murfitt, J. H. Song, H. Y. Hwang, J. Silcox, N. Dellby, and O. L. Krivanek, Science **319**, 1073 (2008).

[7] K. Suenaga et al., Nature Chem. **1**, 415 (2009).

[8] M. B. Sadan, L. Houben, S. G. Wolf, A. Enyashin, G. Seifert, R. Tenne, and K. Urban, Nano Lett. **8**, 891 (2008).

[9] J. C. Meyer et al., Nature Mater. **10**, 209 (2011).

[10] S. Iijima, Nature (London) **354**, 56 (1991).

[11] S. Iijima and T. Ichihashi, Nature (London) **363**, 603 (1993).

[12] H. W. Kroto, J. R. Heath, S. C. O'Brien, R. F. Curl, and R. E. Smalley, Nature (London) **318**, 162 (1985).

[13] K. S. Novoselov, A. K. Geim, S. V. Morozov, D. Jiang, Y. Zhang, S. V. Dubonos, I. V. Grigorieva, and A. A. Firsov, Science **306**, 666 (2004).

[14] A. K. Geim and K. S. Novoselov, Nature Mater. **6**, 183 (2007).

[15] D. Pacile, J. C. Meyer, Ç. Ö. Girit, and A. Zettl, Appl. Phys. Lett. **92**, 133107 (2008).

[16] K. S. Novoselov, D. Jiang, F. Schedin, T. J. Booth, V. V. Khotkevich, S. V. Morozov, and A. K. Geim, Proc. Natl. Acad. Sci. U.S.A. **102**, 10 451 (2005).

[17] F. Banhart, Rep. Prog. Phys. **62**, 1181 (1999).

[18] M. W. Lucas and E. W. J. Mitchell, Carbon **1**, 345 (1964).

[19] V. H. Crespi, N. G. Chopra, M. L. Cohen, A. Zettl, and S. G. Louie, Phys. Rev. B **54**, 5927 (1996).

[20] B. W. Smith and D. E. Luzzi, J. Appl. Phys. **90**, 3509 (2001).

[21] A. Krasheninnikov, F. Banhart, J. Li, A. Foster, and R. Nieminen, Phys. Rev. B **72**, 125428 (2005).

[22] A. Zobelli, A. Gloter, C. Ewels, G. Seifert, and C. Colliex, Phys. Rev. B **75**, 245402 (2007).

[23] K. Mølhave, S. B. Gudnason, A. T. Pedersen, C. H. Clausen, A. Horsewell, and P. Bøggild, Ultramicroscopy **108**, 52 (2007).

[24] J. H. Warner, F. Schäffel, G. Zhong, M. H. Rümmeli, B. Büchner, J. Robertson, G. Andrew, and G. A. D. Briggs, ACS Nano, **3**, 1557 (2009).

[25] D. Cherns, F. J. Minter, and R. S. Nelson, Nucl. Instrum. Methods **132**, 369 (1976).

[26] R. F. Egerton, R. McLeod, F. Wang, and M. Malac, Ultramicroscopy **110**, 991 (2010).

[27] R. F. Egerton, Philos. Mag. **35**, 1425 (1977).

[28] W. Zag and K. Urban, Phys. Status Solidi A **76**, 285 (1983).

[29] V. H. Crespi, L. X. Benedict, M. L. Cohen, and S. G. Louie, Phys. Rev. B **53**, R13 303 (1996).

[30] H. Terrones, M. Terrones, E. Hernández, N. Grobert, J-C. Charlier, and P. M. Ajayan, Phys. Rev. Lett. **84**, 1716 (2000).

[31] Mark Lusk and L. Carr, Phys. Rev. Lett. **100**, 175503 (2008).

[32] Michael D. Fischbein and Marija Drndic, Appl. Phys. Lett. **93**, 113107 (2008).

[33] J. Kotakoski, A. V. Krasheninnikov, U. Kaiser, and J. C. Meyer, Phys. Rev. Lett. **106**, 105505 (2011).

[34] A. V. Krasheninnikov and F. Banhart, Nature Mater. **6**, 723 (2007).

[35] J. C. Meyer, C. Kisielowski, R. Erni, M. D. Rossell, M. F. Crommie, and A. Zettl, Nano Lett. **8**, 3582 (2008).

[36] See Supplemental Material at http://link.aps.org/supplemental/10.1103/PhysRevLett.108.196102 for additional data, details of the calculation, and supplementary discussions.

[37] U. Kaiser, J. Biskupek, J. C. Meyer, J. Leschner, L. Lechner, H. Rose, M. Stöger-Pollach, A. N. Khlobystov, P. Hartel, H. Müller, M. Haider, S. Eyhusen, and G. Benner, Ultramicroscopy **111**, 1239 (2011).

[38] J. C. Meyer, C. O. Girit, M. F. Crommie, and A. Zettl, Appl. Phys. Lett. **92**, 123110 (2008).

[39] Hye Jin Park, Jannik Meyer, Siegmar Roth, and Viera Skákalová, Carbon **48**, 1088 (2010).

[40] C. O. Girit, J. C. Meyer, R. Erni, M. D. Rossell, C. Kisielowski, L. Yang, C.-H. Park, M. F. Crommie, M. L. Cohen, S. G. Louie, and A. Zettl, Science **323**, 1705 (2009).

[41] J. Kotakoski, D. Santos-Cottin, and A. V. Krasheninnikov, ACS Nano **6**, 671 (2012).

[42] A. Barreiro, F. Boerrnert, S. M. Avdoshenko, B. Rellinghaus, G. Cuniberti, M. H. Ruemmeli, and L. M. K. Vandersypen, arXiv:1201.3131.

[43] J. Kotakoski, J. Meyer, S. Kurasch, D. Santos-Cottin, U. Kaiser, and A. Krasheninnikov, Phys. Rev. B **83**, 245420 (2011).

[44] N. F. Mott, Proc. R. Soc. A **124**, 425 (1929).

[45] W. McKinley and H. Feshbach, Phys. Rev. **74**, 1759 (1948).

[46] W. L. Brown and W. M. Augustyniak, J. Appl. Phys. **30**, 1300 (1959).

[47] T. Iwata and T. Nihira, J. Phys. Soc. Jpn. **31**, 1761 (1971).

[48] V. K. Tewary and B. Yang, Phys. Rev. B **79**, 125416 (2009).

[49] J. Kotakoski, C. Jin, O. Lehtinen, K. Suenaga, and A. Krasheninnikov, Phys. Rev. B **82**, 113404 (2010).